

Parker Solar Probe evidence for scattering of electrons in the  
young solar wind by narrowband whistler-mode waves

C. Cattell<sup>1</sup>, A. Breneman<sup>1</sup>, J. Dombeck<sup>1</sup>, B. Short<sup>1</sup>, J. Wygant<sup>1</sup>, J. Halekas<sup>2</sup>, Tony  
Case<sup>5</sup>, J. Kasper<sup>4</sup>, D. Larson<sup>3</sup>, Mike Stevens<sup>5</sup>, P. Whittesley<sup>3</sup>, S. Bale<sup>3,10</sup>, T.  
Dudok de Wit<sup>6</sup>, K. Goodrich<sup>3</sup>, R. MacDowall<sup>7</sup>, M. Moncuquet<sup>9</sup>, D. Malaspina<sup>8</sup>, M.  
Pulupa<sup>3</sup>

1. School of Physics and Astronomy, University of Minnesota, 116 Church St.  
SE Minneapolis -mail:cattell@umn.edu

2. Department of Physics and Astronomy, University of Iowa, Iowa City, IA  
52242, USA

3. Space Sciences Laboratory, University of California, Berkeley, CA 94720-  
7450, USA

4. Climate and Space Sciences and Engineering, University of Michigan, Ann  
Arbor, MI 48109, USA

5. Smithsonian Astrophysical Observatory, Cambridge, MA 02138 USA

6. LPC2E, CNRS and University of Orléans, Orléans, France

7. Solar System Exploration Division, NASA/Goddard Space Flight Center,  
Greenbelt, MD, 20771

8. Laboratory for Atmospheric and Space Physics, University of Colorado,  
Boulder, CO 80303, USA

9. LESIA, Observatoire de Paris, Université PSL, CNRS, Sorbonne Université,  
Université de Paris, 5 place Jules Janssen, 92195Meudon,France

10. Department of Physics, University of California, Berkeley, Berkele

To be submitted to ApJLett

Solar wind (1534), Space plasmas (1544), Interplanetary physics (827), Interplanetary turbulence (830, Plasma astrophysics (1261)

Running title: Scattering of strahl by narrowband whistlers

**Abstract:** Observations of plasma waves by the Fields Suite and of electrons by the Solar Wind Electrons Alphas and Protons Investigation (SWEAP) on Parker Solar Probe provide strong evidence for pitch angle scattering of strahl-energy electrons by narrowband whistler-mode waves at radial distances less than  $\sim 0.3$  AU. We present two example intervals of a few hours that include 8 waveform captures with whistler-mode waves and 26 representative electron distributions that are examined in detail. Two were narrow; 17 were clearly broadened, and 8 were very broad. The two with narrow strahl occurred when there were either no whistlers or very intermittent low amplitude waves. Six of the eight broadest distributions were associated with intense, long duration waves. Approximately half of the observed electron distributions have features consistent with an energy dependent scattering mechanism, as would be expected from interactions with narrowband waves. A comparison of the wave power in the whistler-mode frequency band to pitch angle width and a measure of anisotropy provides additional evidence for the electron scattering by whistler-mode waves. The pitch angle broadening occurs in over an energy range comparable to that obtained for the  $n=1$  (co-streaming) resonance for the observed wave and plasma parameters. The additional observation that the heat flux is lower in the interval with multiple switchbacks may provide clues to the nature of switchbacks. These results provide strong evidence that the heat flux is reduced by narrowband whistler-mode waves scattering of strahl-energy electrons.

## 1. Introduction

Whistler-mode waves have long been proposed as a potential mechanism for scattering of solar wind electrons. Many previous theoretical arguments indicated that the waves must propagate sunward to match the resonance condition for waves propagating parallel to the interplanetary magnetic field (Vocks et al., 2005; Saito and Gary, 2007). Several studies have presented evidence for parallel propagating whistler-mode waves (Lacombe et al., 2014; Stansby et al., 2016; Tong et al., 2019); however, only few examples of waves propagating sunward have been found (Agapitov et al., 2020; Cattell et al., 2021a). Although most theoretical and simulation studies have assumed parallel propagation, Pistinner and Eichler (1998) examined the role of obliquely propagating whistlers, and concluded that they can control the electron heat flux. Electric field waveform captures from STEREO at 1 AU provided evidence that large amplitude narrowband whistlers were frequently obliquely propagating, enabling resonant interactions with electrons without the need for sunward propagation (Breneman et al., 2010; Cattell et al., 2020). Similar obliquely propagating whistler-mode waves are observed by Parker Solar Probe (PSP) inside  $\sim 0.3$  AU (Cattell et al., 2021a; Agapitov et al., 2020).

Many possible instability mechanisms have been proposed, including temperature anisotropy (Gary and Wang, 1996), heat flux instabilities (Forslund, 1970; Feldman et al., 1975; Gary, 1978; Gary et al., 1975; Shaaban et al., 2018), heat flux fan instability (Bošková et al., 1992; Krafft and Volokitin, 2003; Vasko et al., 2019; oblique heat flux whistler/fast magnetosonic instability (Verscharen et al., 2019); and electron beam instabilities (Sauer and Sydora, 2010). A number of studies have examined electron properties, to determine instability mechanisms for the observed whistlers (Lacombe et al., 2014; Stansby et al., 2016; Tong et al., 2019). One likely mechanism for generating the oblique waves observed in the STEREO (Cattell et al., 2020), and Parker Solar Probe (Cattell et al. 2021a) waveform capture data is the heat flux fan instability. The electron beam mechanism might operate also, but the necessary beams have not been observed. Agapitov et al. (2020) concluded that temperature anisotropy in concert with magnetic field gradients might destabilize whistlers observed by PSP. A few authors have made direct comparisons of whistlers and electron distributions for evidence of scattering by the waves. Kajdič et al. (2016) found that strahl

electron distributions were broader when parallel propagating whistlers were observed when compared to intervals without waves. Gurgiolo et al. (2012) showed that halo electrons were scattered from the strahl, but did not see any evidence of the type of waves needed to provide the scattering.

Evolution of the electron distributions has been examined using data from satellites at radial distances from the Sun ranging from Parker Solar Probe inside  $\sim 0.2$  AU (Halekas et al., 2020a, 2020b) to Ulysses at  $\sim 4$  AU (Štverák et al., 2009). These observations are consistent with the existence of significant wave scattering in addition to collisional effects (Maksimovic et al., 2005; Štverák et al., 2009; Wilson III et al., 2000). Halekas et al. (2020b) have shown that, at distances of  $0.125$ – $0.25$  AU, the electron heat flux measurements are most consistent with the fan instability (Vasko et al., 2019) and/or the oblique fast magnetosonic/whistler instability (Verscharen et al. 2019).

In this letter, we present the first direct evidence for scattering of solar wind electrons by narrowband whistler-mode waves at distances less than  $0.3$  AU from the Sun. Statistical properties of these waves were presented by Cattell et al. (2021a). Data sets are presented in section 2. Overviews of two intervals showing wave spectra, electric and magnetic field waveforms, and electron pitch angle data, and a set of shorter intervals with electron distributions are presented in section 3. Discussion and conclusions are given in section 4.

## 2. Data sets and overview

We utilize data from the Parker Solar Probe Fields (Bale et al., 2016) and Solar Wind Electrons Alphas and Protons Investigation (SWEAP) (Kasper et al., 2016) instrument suites. From FIELDS (Bale et al., 2016), we utilize the Level 2 waveform capture data for the three electric field components and the three search coil magnetic field components obtained during the first solar encounter. The waveform data utilized in this study were obtained for  $\sim 3.5$  s intervals at  $\sim 150$  ksamples/s. Storage and transmission of these data was controlled by a quality flag, and in the first encounter dust impacts often triggered the quality flag. Therefore, the waves observed in this data set are often not the largest that occur. To examine the duration of the whistler-mode wave activity, we show one electric field and one magnetic field channel in the DC coupled bandpass filter (BPF) data which is obtained at a cadence of 1 spectrum every  $\sim 1.7$  s, over a frequency range from  $0.4$  Hz to  $4000$  Hz. We also

show one electric field and one magnetic field channel in the DC coupled spectral data, which is obtained at a rate of 1 spectra every ~28 seconds, over a frequency range of ~10 Hz to 4.8 kHz (Malaspina et al., 2016). The Level 2 quasi-static magnetic field data in RTN (radial-tangential-normal) coordinates at ~4 samples per second are used for determining pitch angles and the background magnetic field structure.

The electron parameters were obtained from the SWEAP Solar Wind Electrons Alphas and Protons Investigation (Kasper et al., 2016) Solar Probe Analyzers (SPAN-A-E and SPAN-B-E)(Whittlesey et al. 2020). We show pitch angle distributions for energies from ~20 to 2000 eV, covering core, halo and strahl (Halekas et al., 2020a; Halekas et al., 2020b). A complete energy-angle scan is obtained in .256 Cy (~.87 s), which are summed on board to obtain a distribution every ~28 s. The solar wind velocity, used to transform distributions into the plasma frame, was obtained from the Level 2 Solar Probe Cup (SPC) moments (Case et al., 2020). For some intervals, we also show heat flux. The solar wind density, and electron core and nonthermal temperatures were obtained from the Fields Quasi-thermal Noise (QTN) data (Moncuquet et al., 2020).

### 3. Observations of whistlers and electron scattering

Figure 1 presents an overview of one interval that contains large amplitude narrowband whistler-mode waves (2018 November 2 from 11:10 to 13:10 UT) that we will discuss in detail. Two different waves types are clearly distinguishable in the electric field (panel a) and magnetic field (panel b). The waves at harmonics of the electron cyclotron frequency ( $f_{ce}$ ), intermittently from ~11:10 to 11:50 UT and again at ~12:16 and 12:24 UT in panel a, have been identified as electrostatic whistler/Bernstein waves seen primarily in regions of quiet radial magnetic field (Malaspina et al., 2020). The electron pitch angles are narrowly field-aligned as expected for strahl, indicating that these waves do not strongly scatter electrons at these energies (panels d, e and f). Note that both the electric field spectrum and the waveform capture 2 indicate that much weaker electron Bernstein waves occurred simultaneously with the whistlers around 1229 UT. The whistler waves, observable in panels a and b from ~12:25 to ~12:37 at  $\sim 0.1 f_{ce}$ , occur when the magnetic field is more variable and usually smaller. Strong scattering at energies from ~200 to ~800 eV is seen in association with the most intense whistler waves from ~1227 to ~1231 UT. Scattering at the lower energies continues in concert with the weaker waves. This association provides strong

evidence for scattering of strahl-energy electrons by narrowband whistlers. Panel g, which plots a comparison of electron heat flux (blue) to the Vasko et al. (2019) heat flux fan instability limit (red), is consistent with whistler regulation of the heat flux. The most intense waves are associated with increases in the core electron temperature, and increases in the plasma density.

Figure 2 presents an example of repetitive correlated electron scattering and whistler waves that occurs within magnetic field ‘switchbacks’ (Bale et al., 2019; Kasper et al., 2019; Dudok de Wit et al., 2020; Horbury et al., 2020). Note that in the region of radial field between switchbacks weaker electrostatic waves at harmonics of  $f_{ce}$  (like those seen in the first ~30 minutes of Figure 1) sometimes occur (Malaspina et al., 2020). The signature of the switchbacks is clearly seen in panel c, which plots the R component of the magnetic field (red) with the R component of the ion flow over-plotted in blue. Note that 300 km/s has been subtracted from the flow to more clearly show the variations. The radial field (in red) rapidly changes from negative ~50 nT to positive values and then back, for example at ~925 UT, ~933 UT, ~939 UT and ~948 UT, correlated with an increase in the flow velocity. Whistler waves (seen in panels a and b) often fill the switchbacks, and electrons are strongly scattered. Wave amplitudes are not as large within the switchbacks, as they are later in the event (~10:18 to 10:45 UT), when the five waveform captures were obtained and the waves are also higher frequency. After ~10:45 UT, when the magnetic field is less variable, there are no whistler waves and the electrons are strongly field-aligned. In the intervals with strong whistlers, the electron distributions are broadened in pitch angle. In contrast to the event in Figure 1, the heat flux is sometimes below the Vasko et al. (2019) fan instability limit, most often within the switchbacks when the whistlers are intense, and the heat flux is lower. As in the previous example, increases in the core electron temperature are observed with the most intense waves. In several cases, the temperature increased from ~25 eV to ~40 to 60 eV, suggesting that the waves may also heat core electrons.

Understanding the nature of the scattering process requires examination of the electron distribution functions, and the waveforms and the wave angles. Panels 1 through 3 in Figure 1 plot one component of the electric field waveform and one of the magnetic field waveform, for each of the three waveform captures obtained during this time period on 2018 November 2. The waveforms are coherent and large amplitude (~5–15 mV/m, and 4 – 7 nT, dB/B~0.1). The wave vectors are variable, from ~5° to 45°. Panels 1 through 6 of Figure 2 plot one component of the five electric field waveforms obtained in this interval

on 2018 November 3. Figure 2, panel 1, which plots the entire 3.5 s waveform capture, illustrates the wave packet structure and variability often seen in the narrowband whistlers; the waveform for one packet is shown in panel 2. The waveforms in panels 2, 4, 5 and 6 are coherent; the example in panel 3 is more non-linear and, in addition, has the signature of higher frequency waves (also seen in Figure 1h). Both the five wave captures and the comparison of power on the electric and magnetic components in the BPF data indicated that the wave propagation vector angles are variable. At times angles are oblique, close to the resonance cone, resulting in significant longitudinal electric fields, as well as a component parallel to the background magnetic field, and at times, the waves propagate close to the magnetic field.

The waveform capture data show that the whistler wave packets vary on sub-second time scales. The  $\sim 28$ s averaged spectral data provide a reasonable estimate of wave occurrence and amplitudes, especially for the longer-lasting and more intense waves, but, as expected, miss the highly variable nature of the waves that is clear in waveforms and in the BPF data. The waveforms in Figure 2 show that individual wave packets can have durations of  $\sim 0.1$  s. The electron distributions have the same  $\sim 28$  s cadence as the spectral data, and are, therefore, averages over regions that could include strong waves interspersed with weak or no waves. For this reason, we would not expect a one-to-one correspondence between the pitch angle broadening and wave amplitudes. In addition, electrons may have interacted with waves upstream of the observations. Utilizing the complementary information provided by high time resolution BPF data and the better frequency resolution spectral data, and a technique developed to study whistler-mode waves in the radiation belts (Tyler et al., 2019a, 2019b), both the frequency and peak power of the whistler-mode waves can be more accurately determined at the higher time resolution. The width of the electron distribution was assessed in two different ways. Because there are cases of very broad distributions (see examples in Figure 4, panels g and h) when the peak flux is not at  $180^\circ$  (away from the sun), the pitch angle width was defined to be the width at half height between the maximum flux (using the actual pitch angle measurement for non- $180^\circ$  peaks or the splined value at  $180^\circ$  pitch angle if  $180^\circ$  is the peak flux) and the minimum flux. Note that the plotted values are full-widths. The second method is an 'anisotropy,' defined to be the measured maximum flux over the minimum flux between  $90^\circ$  and  $180^\circ$  degrees. When the strahl is narrowly peaked, the 'anisotropy' is large; when the distribution is very broad, the anisotropy is very small. Figure 3 plots the pitch angle width and 'anisotropy' for the energy band centered at 314 eV versus the magnetic power in the whistler-mode

frequency band for the two days containing the shorter intervals shown in Figures 1 and 2. The median value for the power is indicated by the red squares; upper quartile ( 75%) and lower quartile ( 25%) are indicated by the red diamonds. It is clear that the narrowest pitch angle distributions (<40° full width, or 20° half width, corresponding large ‘anisotropies,’ are on average associated with the lowest wave power. The broadest distributions (large pitch angle width and small anisotropy) are clearly correlated with the largest amplitude waves.

Energy-pitch angle distributions of the electrons provide more detailed diagnostics for the interactions with the whistler waves. Figure 4 presents examples of the types of distributions observed. Times given are the center time of the 28 s interval. Note that energies below 20 eV are not included due to possible spacecraft effects. Panels a and b are narrow and field-aligned over energies of ~100 eV to 1 keV, consistent with strahl. Comparison to Figure 1 shows that no whistler-mode waves were observed at the time of the distribution in panel b, and very weak waves at the time of the one in panel a. The broadening of the pitch angles seen in panels c, d and e is energy-dependent, primarily between ~250 and 600 eV. The case in panel e is broader at low energies. In contrast, the cases in panels f, g and h have wide pitch angle distributions over the range from < 100 eV to ~1 keV, although the extent of the broadening varies significantly. At some The extreme broadening seen in Figure 4h (2018 November 2 12:30:11 UT) which extends to lower energies is not a unique case; at least two other distributions (12:25:03 UT, 12:27:51 UT) are nearly identical. The three waveform captures (Figure 1) were obtained at this time, and the large amplitudes continue for adjacent times as can be inferred from the BPF data. Similarly the very broad distribution in Figure 4g on 2018 November 3 is similar to ones at 10:15:04 UT and 10:43:58 UT. The occurrence of peaks that are not at 180° in some energy bands (seen most clearly in panels g and h, but also observable at high energies in d and e) is consistent with the results of our particle tracing code (Vo et al., 2020; Cattell et al., 2021b).

Table 1 presents a qualitative relationship between the whistler-mode wave amplitudes and durations and the twenty-six representative energy-pitch angle distributions (categorized as narrow, broadened and very broad, as discussed above) that were obtained when the distributions were not be impacted by rapid changes in the magnetic field (13 on 2018 November 2, and 13 on 2018 November 3). As discussed above, a perfect correlation would not be expected because the obliquity of the waves varies, the electrons may have interacted with waves upstream of the observation location, and due to the mismatch

between wave packet and distribution function timescales. Waves at the time of each distribution were categorized as: (1) very intense (BPF electric field amplitude  $>4 \times 10^{-4}$  V, BPF magnetic field  $>.05$  nT, spectral electric field  $>1 \times 10^{-8}$  V $^2$ /Hz and spectral magnetic field  $>5.0 \times 10^{-4}$  nT $^2$ /Hz, in the appropriate frequency band); (2) intense (meeting criteria for very intense for only part of the interval, or only for the BPF or the spectra, or occurring in all channels at reduced intensity); (3) moderate (occurring for part of interval with reduced intensities(BPF electric field amplitude  $>1.5 \times 10^{-4}$  V, BPF magnetic field  $>.015$  nT, spectral electric field  $>1 \times 10^{-9}$  V $^2$ /Hz and spectral magnetic field  $>1.0 \times 10^{-5}$  nT $^2$ /Hz, in the appropriate frequency band); (4) waves detected only in the electric field; and (5) very weak, intermittent waves or no detectable waves. Table 1 summarizes the comparison of distribution characteristics and wave amplitudes, which can also be inferred from Figure 3. Of the two narrow distributions (blue arrows), the narrowest, Figure 4b, occurred when the waves were below the threshold, and Figure 4a occurred when the waves were very weak, and intermittent. Distributions that have evidence of pitch angle scattering usually occur with moderate or large whistler waves; 15 broad (orange) or red (very broad) distributions are simultaneous with intense (2) or very intense (1) whistlers, and 5 with moderate (3) waves. These results clearly show that the whistler-mode waves scatter electrons on the  $\sim$ 100 eV to  $\sim$ 1keV range. Comparison of distributions that are closely spaced in time suggests that increases in pitch angle may sometimes be associated with decreases in energy.

#### 4. Discussion and conclusions

The intervals shown above provide strong evidence for scattering of solar wind electrons at energies of  $\sim$ 100 eV to  $\sim$ 1 keV by narrowband whistler-mode waves. This is consistent with the results of a particle tracing code (Vo et al., 2020) for wave and plasma parameters based on 1 AU measurements (Breneman et al., 2010).

The intense narrowband whistlers occur primarily in regions where the solar wind magnetic field is variable and often weaker, and in association with magnetic switchbacks, as also reported by Agapitov et al. (2020). Statistics on narrowband whistlers inside  $\sim$ .3 AU (Cattell et al., 2021a) also confirm this association. In several of the events we showed above, although the whistlers are strongest near the edges, intermittent weaker waves fill the entire switchback. The occurrence of intense whistlers and electron scattering

within switchbacks may aid in understanding their origin. We calculated the resonant energies for the observed wave frequencies, wave angles, background magnetic field, and density using the whistler dispersion relation, and the resonance condition,  $\omega - \vec{k} \cdot \vec{v}_e = n\Omega_e$ , where  $\omega$  is the wave frequency,  $\vec{k}$  is the wave vector,  $\vec{v}_e$  is the electron velocity and  $\Omega_e$  is the electron gyrofrequency. We include the Doppler shift of the wave frequency and the electron velocity relative to the solar wind flow. For our events, the ratio of our measured frequencies to the electron gyrofrequency is  $\sim 0.1$ . The wave phase velocity can be estimated from the measured  $\partial E / \partial B$  ratios, which range from  $\sim 2000$  km/s to  $\sim 7000$  km/s, larger than the solar wind speeds of  $\sim 250$  to  $350$  km/s. For cases where  $\vec{k} \cdot \vec{v}_e$  is positive, resonant energies for  $n=1$  range from  $\sim 300$  to  $\sim 700$  eV; for  $\vec{k} \cdot \vec{v}_e$  less than zero ( $n=-1$ ), resonant energies are higher,  $\sim 1000$  to  $1400$  eV. For the Landau resonance,  $\frac{\omega}{k_{\parallel}} = v_{e\parallel}$ , the resonant energies range from 10s of eV to 100s of eV, which could explain the broadening seen at the lower energies. It might also be associated with the increase in core electron temperature seen in association with the largest whistlers. This core heating was also observed in a statistical study of whistler waves observed by PSP (Cattell et al., 2021). More often the scattering we observe, and in particular, the energy dependent scattering is consistent with the  $n=1$  (co-streaming) case.

With the assumption that the waves are parallel propagating, many authors have shown that scattering rates are proportional to  $\Omega_e \delta B^2 / B^2 \propto \delta B^2 / B$  (Brice, 1964; Kennel and Petschek, 1966; Lyons et al., 1972, and Albert, 2017, for whistlers in the context of radiation belt; Kulsrud, 2005, for Alfvén waves in the solar wind). The approach used is often based on the relationship between the pitch angle change and energy change. An analogous argument can be made for oblique waves by transforming into the de Hoffmann-Teller frame rather than the wave frame, because in this frame the wave propagates along the magnetic field. This ratio is largest for the waveform captures at 10:19:15 and 10:43:47 on 11-3-2018 (both close to very broad distributions), and somewhat smaller for 10:30:29 on 11-3-2018 and 12:27:57 and 12:30:05 on 11-2-2018 (all near broad distributions). Although this is not a statistically significant number of events, it is consistent with the scaling of the scattering rate and with the statistical results obtained as in Figure 3 (not shown).

Our results are consistent with the conclusions of Halekas et al. (2020b) that the electron heat flux is regulated by the whistler fan and/or oblique

fast magnetosonic/whistler modes. We show, for the first time, that the strahl energy electrons, which carry the heat flux, are strongly scattered by the oblique narrowband whistler-mode waves, thus reducing the heat flux. The same wave mode is observed at 1 AU by STEREO (Cattell et al., 2020a; Breneman et al., 2010), and, at this distance from the Sun, the heat flux fan instability is also the most likely wave generation mechanism. These waves are, therefore, the most likely candidates for regulating the electron heat flux and scattering of strahl electrons into the halo.

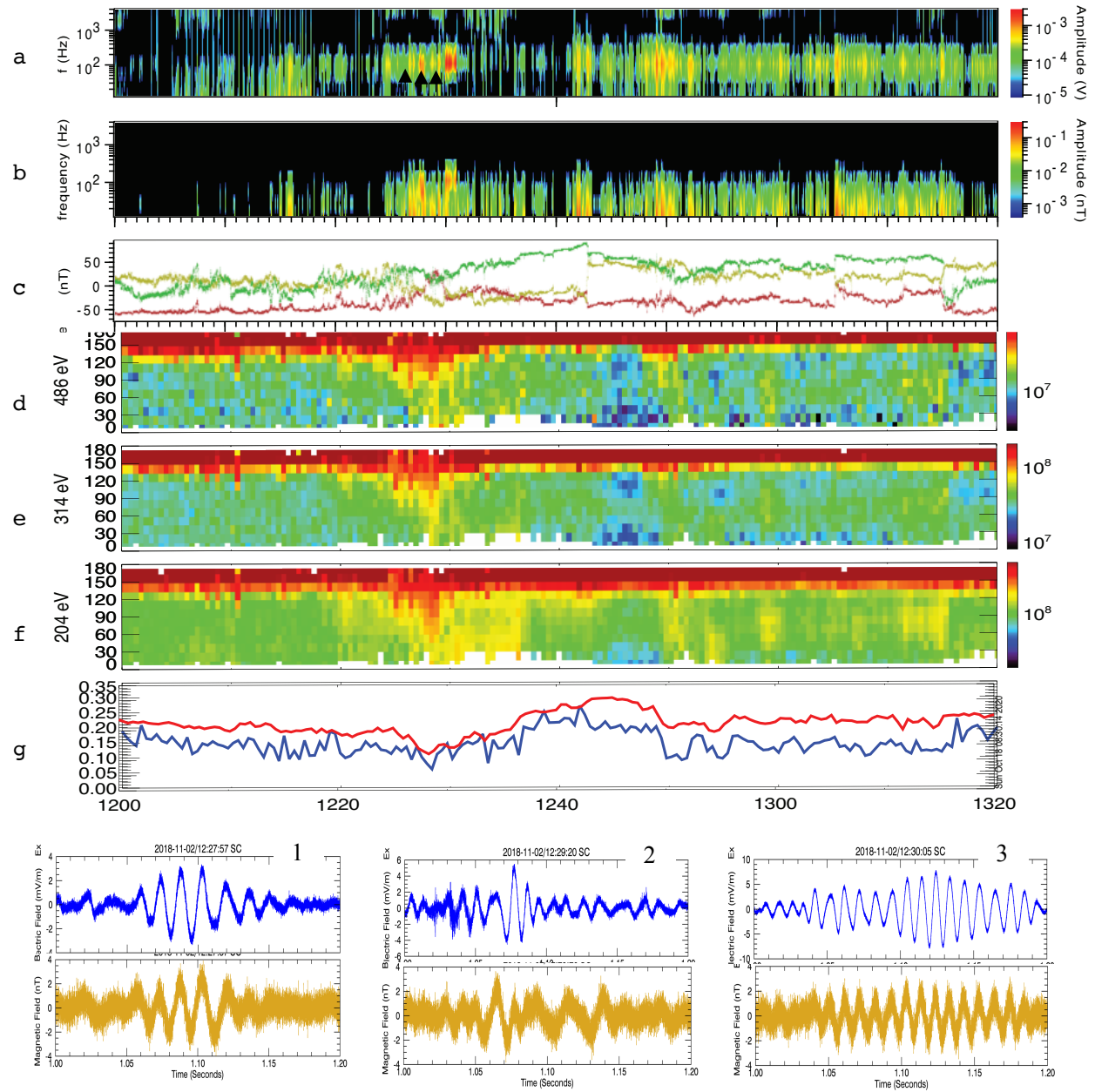
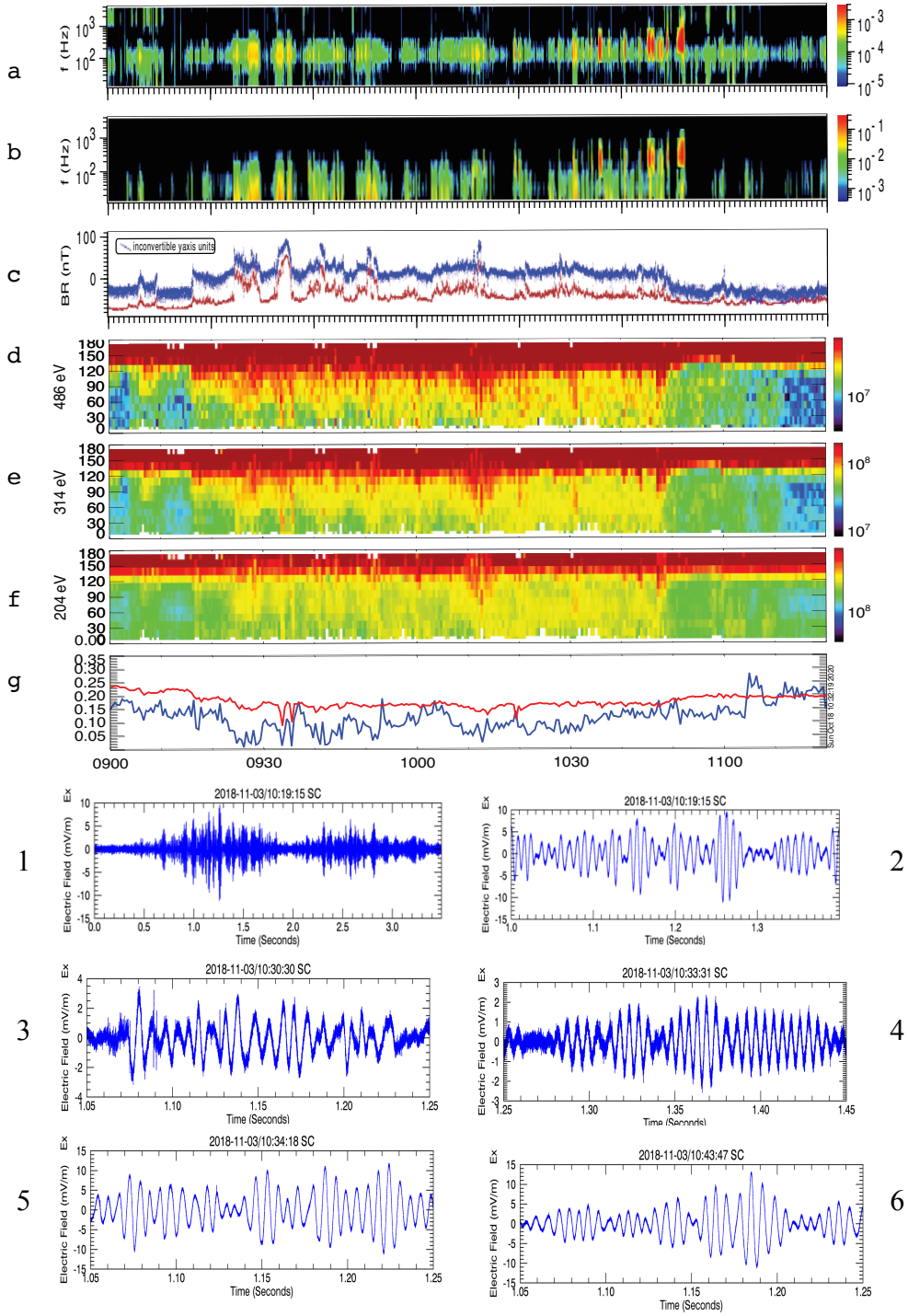


Figure 1. November 2, 2018 from 12:00 to 13:20. From top to bottom: DC coupled electric field BPF spectrum from 4 Hz to 4 kHz; DC coupled magnetic field BBF spectrum from 4 Hz to 4 kHz; the magnetic field in RTN coordinates; electron pitch angle spectra for center energies of 486 eV, 314 eV, and 205 eV; normalized heat flux(black) and heat flux fan instability threshold (red). Bottom panels: 0.2 s snapshots from the three waveform captures obtained during this interval, Ex (blue) and Bz (gold).



**Figure 2.** Parker Solar Probe observations of waves, solar wind and electron distributions. From top: DC coupled electric field and search coil magnetic field BPF spectra (12 Hz to 4000 Hz); R(radial) component of the magnetic field (red) with the R component of the ion flow velocity (with 300 km/s subtracted) in blue; pitch angle spectra for electrons with center energies of 751 eV, 314 eV, 204 eV and 132 eV; normalized heat flux (black) and fan instability threshold (red); one full 3.5 s waveform, and five 0.2 second snapshots of the SC-X component of the electric field from the five 3.5 s burst waveform captures transmitted during this interval.

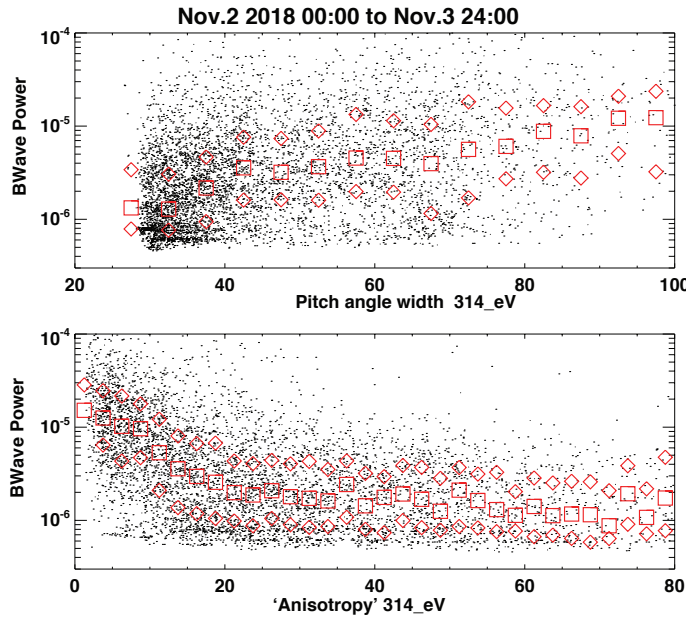


Figure 3. Scatter plot of whistler wave power (magnetic field) versus pitch angle width and 'anisotropy'- defined as the measured maximum flux over the measured minimum flux between 90 degrees and 180 degrees for the two days containing the time intervals in Figure 1 and 2. The median values of the wave power are over-plotted as red squares, and the upper 75% and lower 25% are over-plotted as red diamonds.

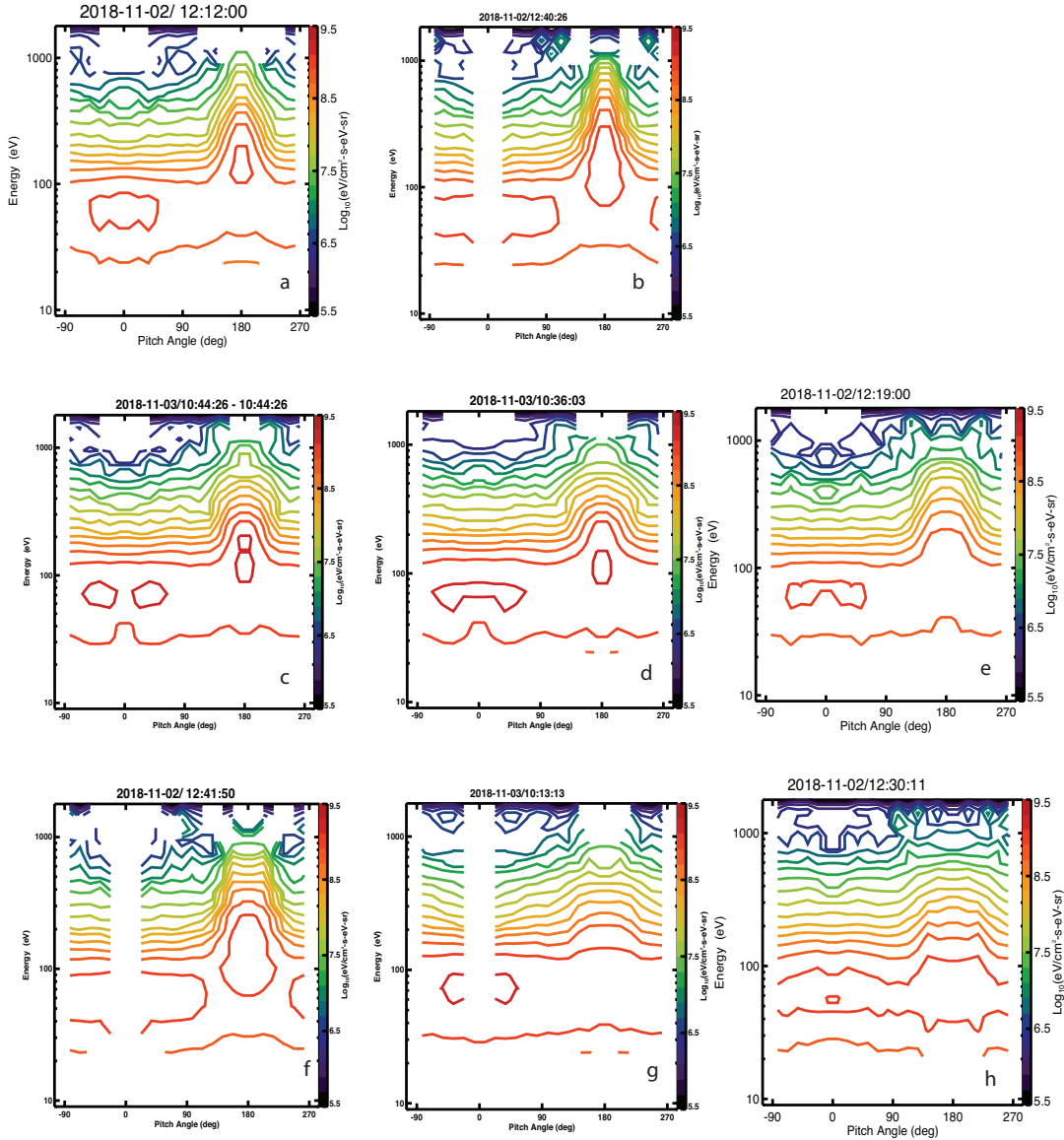


Figure 4. Examples of types of electron energy-pitch angle distributions observed during the intervals shown in Figures 1 and 2. Panels a and b: Narrow strahl distributions; panels c, d and e: energy dependent broadening; and panel f: energy independent broadening; panels g and h: extreme broadening with peaks off 180 degrees.

Wave DF	5	4	3	2	1	(1+2)
narrow	2					
broad		4	2	6	5	11
Very broad			2	2	4	6

Table 1. Qualitative comparison of electron distribution and wave properties. Narrow, broad and very broad refer to electron pitch angle widths, as described in the text. 1,2,3, 4 and 5 refer to wave characteristics, with 1 being the most intense, 4 having only electric field signatures, and 5 having very weak and intermittent or no waves. See text for details.

**Acknowledgements:** We acknowledge the NASA Parker Solar Probe Mission, the FIELDS team led S. D. Bale, and the SWEAP team led by J. Kasper for use of data. The FIELDS and SWEAP experiments on the Parker Solar Probe spacecraft were designed and developed under NASA contract NNN06AA01C. Data analysis at was supported under the same contract.

## REFERENCES

Agapitov, O. V., Wit, T. Dudok de, Mozer, F. S. et al., 2020, *ApJ*, 89, L20

Albert, J. M., 2017, *JGRA*, 122, 5339–5354, doi:10.1002/2017JA024124.

Bale S. D., Badman S. T., Bonnell J. W. et al, 2019, *Nature* **576** 237

Bale S. D., Goetz K., Harvey P. R. et al 2016 *Space Sci. Rev* **204** 49

Berčič, L, M Maksimović, S Landi, L Matteini, 2019, *MNRAS* 486, 3

Bošková, J., Tříška, P., Omelchenko, Y.A. et al. 1992, *Stud Geophys Geod* **36**, 177–187

Breneman A., Cattell C., Schreiner S. et al 2010 *JGRA* **115** A08104

Brice, N., 1964, *JGR*, 69( 21), 4515– 4522, doi:[10.1029/JZ069i021p04515](https://doi.org/10.1029/JZ069i021p04515).

Case, A.W., Kasper, J. C., Stevens, M. L., et al. 2020, *ApJS*, 246, 43

Cattell, C., Short, B., Breneman A.W. & Grul P., 2020, *ApJ* **897** 126

Cattell, C. et al., 2021a, *Astronomy and Astrophysics*, AA/2020/39550, in press.

Cattell, C., T. Vo, A. Breneman, R. Lysak, T. Jones, A. West 2021b, Nonlinear interactions of narrowband large amplitude whistler-mode waves with electrons in the solar wind, in prep.

Dudok de Wit, Thierry et al 2020 *ApJS* **246** 39

Gurgiolo, C. and M. Goldstein, 2016, *Ann. Geophys.*, 34, 1175–1189, doi:10.5194/angeo-34-1175-2016

Halekas J. S., Whittlesey P., Larson D. E., McGinnis D., Maksimovic M., et al., 2020a, *ApJS*, 246, 22

Halekas, J. S. P. L. Whittlesey, D. E. Larson, D. McGinnis, S. D. Bale et al.,  
A&A, in press, 2020b

Horbury Timothy S. et al 2020 *ApJS* **246** 45

Kajdič, P., Alexandrova, O., Maksimovic, M., Lacombe, C., Fazakerley, A.N., 2016.  
*ApJ*, 833, 172

Kasper J. C., Abiad R., Austin G. et al 2016 *Space Sci. Rev* **204** 131

Kasper, J. C., Bale, S. D., Belcher, J. W., et al. 2019, *Nat*, 576, 228

Krafft, C. and Volokitin, A.: 2003, *AnGeo*, 21, 1393–1403

Lacombe, C., Alexandrova, O., Matteini, L., Santolík, O., Cornilleau-Wehrlin, N.,  
Mangeney, A., de Conchy, Y., Maksimovic, M., 2014, *ApJ*, 796

Kulsrud, Russell, 2005, *Plasma Physics for Astrophysics*, ISBN-10: 0691120730

Lyons, L. R., Thorne, R. M., and Kennel, C. F., 1972, *JGR*, 77, 3455– 3474,  
doi:[10.1029/JA077i019p03455](https://doi.org/10.1029/JA077i019p03455).

Maksimovic, M., et al., 2005, *JGR*, 110, A09104

Malaspina, D., Ergun, R. E., Bolton, M., et al. 2016, *JGRA*, 121, 5088

Malaspina D., Halekas, Laura Berčič et al 2020 *ApJS* **246** 21

Moncuquet Michel, Meyer-Vernet Nicole, Issautier Karine, Pulupa Marc, Bonnell  
J.W., et al., 2020,

Pistinner, S. L. and D. Eichler, 1998, *Mon. Not. R. Astron. Soc.* 301, 49–58

Saito, S., and S. P. Gary, 2007, *Geophys. Res. Lett.*, 34, L01102,  
doi:[10.1029/2006GL028173](https://doi.org/10.1029/2006GL028173).

Sauer, K., and R. D. Sydora 2010, *AnGeo*, 28, 1317–1325

Stansby, D. et al., 2016, *ApJL*, 829, L16

Štverák, Š., Maksimovic, M., Trávníček, P. M., Marsch, E., Fazakerley, A. N., and Scime, E.E., 2009, *JGR* 114, A05104

Tong, Y. et al 2019 *ApJ* **878** 41

Tyler, E., A. Breneman, C. Cattell, et al., 2019a, *GRL*,  
<https://doi.org/10.1029/2019GL082292>

Tyler, E., Breneman, A., Cattell, C., Wygant, J., Thaller, S., & Malaspina, D., 2019b, *JGR*, 124, <https://doi.org/10.1029/2019JA026913>

Vasko T. et al 2019 *ApJ* **871** L29

Verscharen, D., Chandran, B. D. G., Jeong, S.-Y., et al. 2019, *ApJ*, 886, 136

Vo, Tien, Cattell, Cynthia, West, Aaron and Lysak, Robert, Earth and Space Science Open Archive, <https://doi.org/10.1002/essoar.10505100.1>, 2020.

Vocks, C., Salem, C., Lin, R. P., & Mann, G. 2005, *ApJ*, 627, 54

Whittlesey, P. L., Larson, D. E., Kasper, J. C., et al. 2020, *The Astrophysical Journal Supplement Series*, 246, 74

Wilson III, L. B., Chen, L.-J., Wang, S., et al. 2019, *The Astrophysical Journal Supplement Series*, 245, 24